Plasma-treatment of polymeric carbon nitride for efficient NO abatement under visible light

Zeng, Q., Ni, J., Mariotti, D., Lu, L., Chen, H., & Ni, C. (2022). Plasma-treatment of polymeric carbon nitride for efficient NO abatement under visible light. *Journal of Physics D: Applied Physics*, *55*(35), [354003]. https://doi.org/10.1088/1361-6463/ac782d

Link to publication record in Ulster University Research Portal

Published in:
Journal of Physics D: Applied Physics

Publication Status:
Published online: 22/06/2022

DOI:
10.1088/1361-6463/ac782d

Document Version
Author Accepted version

General rights
Copyright for the publications made accessible via Ulster University's Research Portal is retained by the author(s) and / or other copyright owners and it is a condition of accessing these publications that users recognise and abide by the legal requirements associated with these rights.

Take down policy
The Research Portal is Ulster University's institutional repository that provides access to Ulster's research outputs. Every effort has been made to ensure that content in the Research Portal does not infringe any person's rights, or applicable UK laws. If you discover content in the Research Portal that you believe breaches copyright or violates any law, please contact pure-support@ulster.ac.uk.

Download date: 30/06/2023

Plasma-treatment of polymeric carbon nitride for efficient NO abatement under visible light

Qimiao Zeng [a], Jiupai Ni [a], Davide Mariotti [b], Lanying Lu [c], Hong Chen [a], Chengsheng Ni [a, d] *

a College of Resources and Environment, Southwest University, Beibei, Chongqing, China, 400715

b School of Engineering, Ulster University, Jordanstown Campus, Shore Road, Newtownabbey, Northern Ireland, UK

c Chongqing Technology and Business University, Nan'an district, Chongqing, 400067 China

d National Base of International S&T Collaboration on Water Environmental Monitoring and Simulation in Three Gorges Reservoir Region, Chongqing 400716, China

Email: C.N.: nichengsheg@swu.edu.cn

Abstract

Photocatalysis is considered to be efficient in combatting emission nitrogen oxide (NOx), which is one of the atmospheric pollutants affecting human health. Polymeric carbon nitride (PCN) is a low-cost polymeric photocatalyst with a 2-dimensional structure that is sensitive to the visible sunlight in the solar spectrum, but its photocatalytic efficiency needs to be enhanced for the purpose of pollutant abatement. In this study, PCN was treated using a facile ambient pressure dielectric barrier discharge

(DBD) plasma in air, Ar and Ar-5% H_2 flow. According to the spectroscopic characterization and NO removal tests, the DBD plasma did not destroy the crystal structure of PCN, but improved the separation efficiency of photogenerated charges and enhanced the capacity of NO abatement. The plasma treatment in Ar-5% H_2 showed an optimal removal efficiency of 69.19% and a selectivity for nitrate of 90.51% under visible light irradiation. The hydrogen plasma etched the PCN surface, resulting in more defects (carbon vacancies) and carbonyl group on the surface, while the air plasma was found to increase the suspending –NOx bonding on the surface for the increased NOx emission under illumination. The generation of high-energy electron and reactive radicals in the electrical discharges could cause the surface modification of PCN for efficient photocatalysis.

Keywords: Polymeric carbon nitride; DBD plasma; NO removal; visible light photocatalysis

1. Introduction

Nitrogen oxides (NOx) are hazardous contaminants, originating from the combustion of fossil fuels and are responsible for environmental problems such as acid rain, photochemical smog, haze, and so on [1]. Nitrogen monoxide (NO) as the most common NOx is very stable and cannot be photodegraded directly under visible light irradiation [2]. Semiconductor photocatalysis is a green technology that utilizes sunlight for the decomposition of air pollutants at ambient conditions and can play an important role in environmental applications [3].

PCN has shown application prospects in photocatalysis due to the advantages of a suitable band gap, high chemical stability and unique 2-dimensional (2D) structure [4, 5]. However, the small specific surface area and rapid recombination of photogenerated charges [6, 7] required additional effort to improve the photocatalytic activities. The reported methods of enhancing the photocatalysis of PCN

include metal/nonmetal doping [8, 9], structural regulation [10, 11], vacancies or defects introduction [12, 13], heterojunction construction [14-16] and recombination with semiconductors [17, 18]. As the photocatalytic oxidation of NO is a superficial reaction, the surface modification could be desired to decrease the effort in energy consumption and capital investment for a high removal efficiency and selectivity for the production of nitrate.

Plasma discharges operated at an atmospheric pressure are commonly used to synthesize or surface engineering of a wide variety of materials [19]. DBD is a type of atmospheric pressure plasma discharges and characterized by short-lived micro-discharges across large surface areas [20]. DBDs have been carried out to modify catalysts by tuning the electronic structure, enhancing the hydrophilicity, and promoting the dispersion of the active component or creating a new active phase [21]. The large fluxes of plasma species could lead to changes in surface structure and morphology, and the resultant active site for the catalytic reactions on the surface [22]. In addition, DBD plasma preparation can reduce photo-generated electron-hole recombination and cause more surface defects, which are beneficial to photocatalysis [23]. The surface physical chemical properties are change by adjusting the processing time and input power of plasma to enhance the catalytic activity [24, 25]. Thus far, studies on plasma modified PCN for NO abatement have received sporadic attention, and the effects on the surface properties under different atmosphere have not been reported.

In this work, PCN was treated by DBD under different atmospheres (air, Ar and Ar-5% H_2) to explore the effects on catalyst surface, physicochemical properties and photocatalytic activity. A series of characterizations was used to evaluate the influence of plasma treatment on the surface properties, such as physical characteristics, chemical bonding states, optical and photoelectrochemical properties.

The plasma-treated PCN showed higher removal efficiency under visible light irradiation of NO than the pristine PCN, results from the optimization of the surface properties induced by plasma treatment. Our work demonstrates an effective modification strategy for enhancing the visible light photocatalytic activity of PCN as a popular 2-dimensinal photocatalyst.

2. Experimental

2.1. Catalysts preparation

The pristine PCN was prepared by a thermal polymerization of melamine precursor. 5 g of melamine (chemical pure, KESHI) was calcined at 550 ^{o}C for 4 hours with rate of 5 ^{o}C min^{-1} in a ceramic crucible with a cover in a muffle furnace. The sample taken was ground into yellow powder (noted as PCN-0). 0.3 g of PCN-0 was dispersed in deionized water and the suspension was spread on a quartz plate (diameter of 70 mm, thickness of 2 mm) to prepare a coating. The quartz and the coating was baked in an oven for 15 min at 60 ^{o}C to evaporate the residual water. The DBD plasma reactor consisted of a high voltage power supply (JMAC-P30-20 mA, JEMAN, Dalian, China) and a plasma reactor composed of two parallel circular stainless steel plate electrodes (diameters of 50 mm and 160 mm), a fluororubber O ring (diameter of 105 mm, thickness of 5 mm) and an upper quartz cover (diameter of 110 mm, thickness of 2 mm) between the electrodes (Figure 1). The reactor was not under vacuum, so the humidity was consistent with the atmospheric environment. The discharge plasma was initiated at room temperature in air or at a constant Ar or Ar-5% H_2 flow (100 mL min^{-1}). The feed gas to the DBD plasma reactor was air or Ar, which creates an oxidation or inert atmosphere, respectively. H_2 plasma was used to product strong reducing species [26]. 5% percent of H_2 in Ar was used based on safety considerations. The discharge was sustained with an alternating voltage of 0.7 kV and a

frequency of 9.9 kHz. The DBD process was applied for 30 min to obtain PCN-30 Air/Ar/Ar-H_2. The plasma treated PCN on quartz was directly used for the future characterization unless specified.

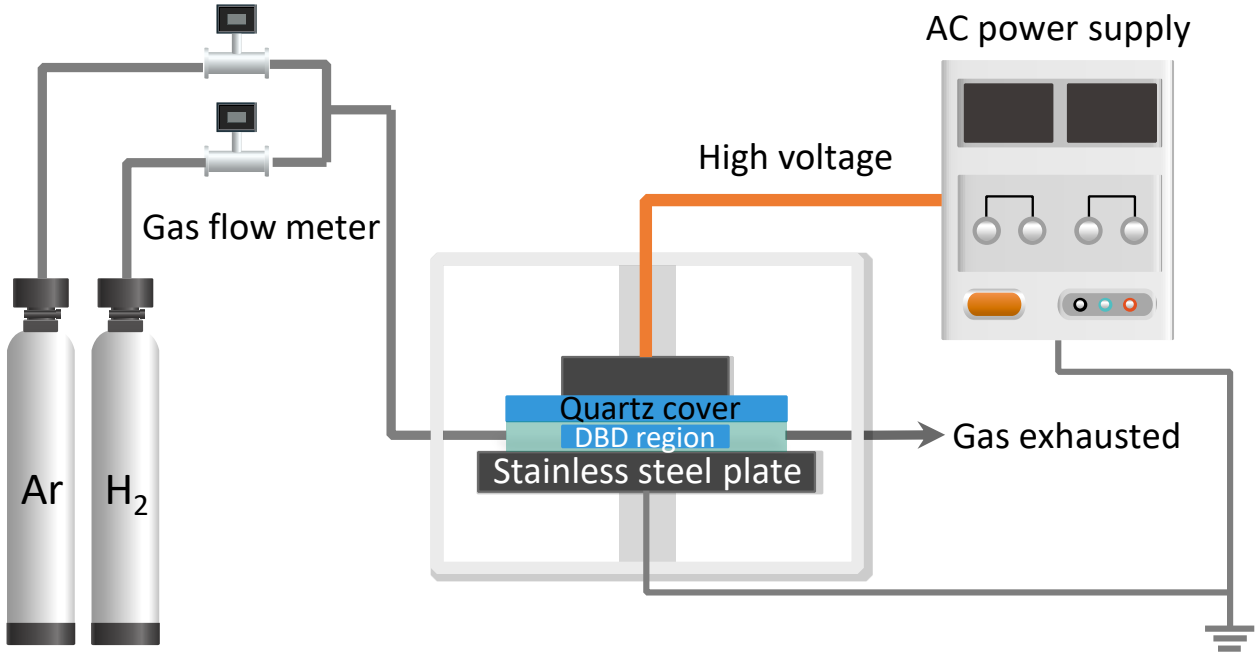

Figure 1. Schematic diagram of the DBD plasma reactor used for the treatment of PCN.

2.2. Characterization

The crystallinity of PCN powder samples scraped from quartz plates was verified by XRD (Persee, XD-3, China) with Cu K_α ray (λ = 1.54178 Å) and their diffraction patterns were measured at an angle of 2θ from 10° to 70°. The morphology and microstructure of the assembled samples were investigated by scanning electron microscopy (SEM, Zeiss Sigma500, Germany). The Brunauer-Emmett-Teller (BET) specific surface areas were analyzed by N_2 adsorption & desorption experiment on an ASAP-2020 (Micromeritics Instrument, USA). The surface of the monolithic photocatalyst was characterized using XPS (ESCALAB 250Xi, USA) using monochromatic Al K_α X-rays (1486 eV) for the overall survey and high-resolution core level of C 1*s*, N 1*s* and O 1*s*. The functional groups and structure of the monolithic

photocatalyst were examined by FTIR (Thermoscientific Nicolet iS20, USA). The total C, H, O and N content was measured on an elemental analyzer for organic materials (ElementarVario Micro Select, ElementarAnalysensysteme, Germany). A commercial fiber-coupled spectrometer (Ocean Optics Inc, USB4000, USA) was used to measure the emission spectra of electronically excited species generated during the DBD treatment. Thermal stability of the reactant and polymer products was carried out using the thermogravimetric analysis (TGA) on a NETSCHZ F3 thermogravimeter (Germany) from room temperature to 800 ^{o}C under flowing air. The equal proportion sample was attached to a small quartz plate (diameter of 23.5 mm, thickness of 2 mm) for DBD treatment, and then directly installed on a UV-1800 spectrometer (MACY, China) to carry out the UV-vis spectra, employing $BaSO_4$ as the reference. Photoluminescence spectroscopy (PL) of the coated samples in air was obtained on a 2D CCD (charge-coupled device) array spectrometer (Control Development, USA) with a 365 nm excitation laser on an integrating sphere. Electron paramagnetic resonance (EPR) signals were recorded with a Bruker A300 spectrometer at room temperature (298 K).

2.3. Photocatalytic NO removal

The photocatalytic experiments of NO removal at ppb levels were performed at ambient temperature in a stainless steel continuous flow reactor with a quartz window of 8 cm in internal diameter. The reactor was fed with mixed air (1 L min^{-1}) and NO (100 ppm in Ar), and the NO gas flow was adjusted to achieve a [NO] of 1 ppm. Humid air was generated by passing the air through a water bath. Flowing water was used to maintain the temperature of the reactor to be around 20 ^{o}C. The NO and NO_2 concentration of the effluent was continuously measured using a NOx analyzer (MIC-600, Eranntex electronics, Shenzhen, China). The reactor was illuminated for 30 min using a light-emitting diode

(LED) lamp (FL, 19-III, 100 W) with photons > 400 nm after 5 minutes' equilibration in the dark.

The NO purification efficiency (η) and selectivity for ionic species (S_i) were defined as follows [27]:

$$\eta = (1 - \frac{[NO]_{out}}{[NO]_{in}}) \times 100\% \quad (1)$$

$$S_i = (1 - \frac{[NO_2]_{out}}{[NO]_{in} - [NO]_{out}}) \times 100\% \quad (2)$$

2.4. Photo-electrochemical measurement

The photocurrent and Mott-Schottky were obtained on an electrochemical workstation (Zennium *Pro*, Zahner, Germany) in a conventional three electrodes configuration with the synthesized samples as the working electrode, a gold mesh as the counter electrode, Ag/AgCl as a reference electrode, and Na_2SO_4 (0.5 M) aqueous solution as the electrolyte, respectively. The working electrodes (2 cm^2) were prepared by spreading a slurry form 5 mg of samples, 25 µL of PEDOT and 50 µL of water on FTO glass with glass rod using adhesive tapes as spacers [28]. After drying in ambient air, the photoelectrodes were dried at 150 ^oC for 30 min. Mott-Schottky was measured using electrochemical impedance spectroscopy (Zannium *Pro*, Zanher, Germany) in the dark condition in a 3-electrode configuration in 1M Na_2SO_4 electrolyte, and the frequency range for the 10 mV sine wave was 1 MHz to 1 Hz. The potential of Mott-Schottky measurement using Ag/AgCl reference was converted to standard hydrogen electrode (SHE) for a comparable analysis with literature.

3. Results

3.1. Optical emissions of the plasma

The optical emission from the plasma relates to specific excited atoms and molecules (Table S1) and the corresponding spectra (Figure 2) are not significantly impacted by the presence of the samples

under flowing air, Ar and Ar-5% H_2. In the air DBD plasma, dominant nitrogen bands and emission from NO are observed in the system along with weak emission from H_α and H_β and O. In the case of Ar, strong OH was found beside the emissions in the spectral range 318–467 nm dominated by N_2 bands [29, 30]. The N_2 bands could be ascribed to the leakage in the setup the release of N from PCN. Strong emissions in the range from 700 nm to 900 nm were mainly attributed to Ar and others in the near UV region were assigned to Ar [31]. The unique peaks for C_2 species (513 nm), H_α (664.6 nm) and H_β (484.1 nm) [32] in the presence of PCN under Ar indicate that there could be C removal from the sample during the plasma treatment. The presence of OH observed in argon and 5% H_2 could induce the replacement of $-NH_2$ group in PCN [33]. The wide emission peak for H_β is very evident as a result of the high H_2 concentration in 5% H_2.

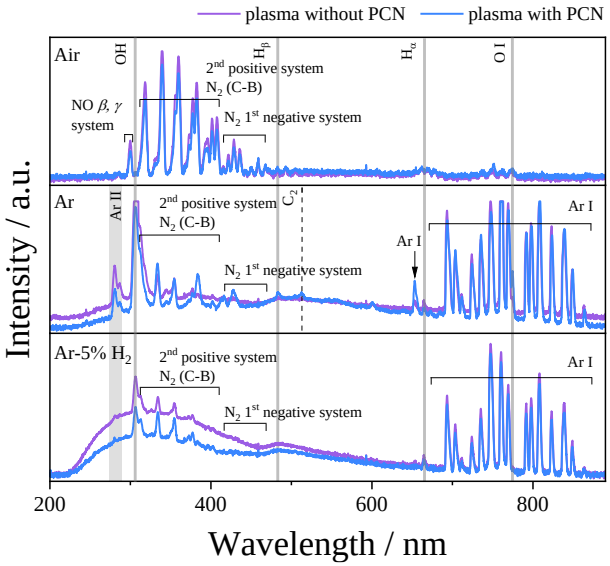

Figure 2. *In situ* optical emission spectra for air, Ar and Ar-5% H_2 plasma (100 mL/min) with and without PCN at room temperature.

3.2. Structure and composition analysis

The XRD (Figure 3(a)) [34] of all samples showed distinct peaks at a 2θ of 12.8° and 27.4° for the (100)

and (002) crystal plane, respectively, indicating that the plasma treatment did not change the crystal structure of PCN. The main peak at around 27.4°, in the inset of Figure 3(a) and corresponding to an interlayer distance of the tri-s-triazine layer [35, 36], shows a shift to high angle direction as a result of the decrease in corresponding interlayer spacing [37]. The *d*-spacing of the (100) plane (Figure 3(b)) [38] was found to expand with the plasma treatment while the one of (002) plane shrank during the treatment [39]. The variation in the *d* spacing could be the creation of carbon vacancies during the plasma treatment. [40]

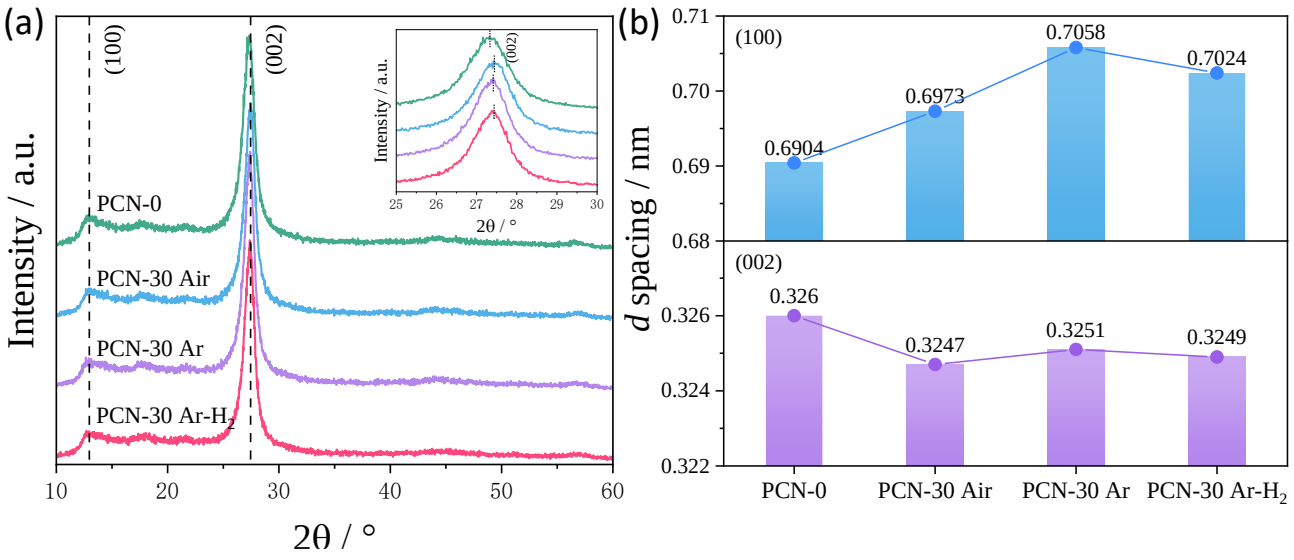

Figure 3. (a) XRD patterns for the pristine and plasma-treated PCN; (b) the corresponding *d*-spacing of the (100) and (002) crystal plane calculated from XRD.

The BET surface area (S_{BET}) of PCN-0 is 22.61 m^2/g and slightly decreased under DBD plasma treatment: 17.16, 22.39 and 18.96 m^2/g for PCN-30 in air, Ar and Ar-5% H_2, respectively. As the S_{BET} is measured on the powdered sample, while the plasma would be more intense effect on the superficial layer of the coating, SEM images (Figure 4) of the surface of the coating could be more representative of the effect of plasma. The morphology of PCN-0 is composed of agglomerates of stacked blocks with

irregular pores inside. The DBD plasma increased the pore size under Ar plasma while the plasma in air or 5% H_2 created fine particles or sheets on the surface of large plates. As there are reactive species, i.e. oxygen and hydrogen in air and 5% H_2, respectively, which caused the polishing of the surface layer for the fine particles, while the hot electrons in Ar plasma would cause the polymerization of the PCN for larger particles only and smaller surface area.

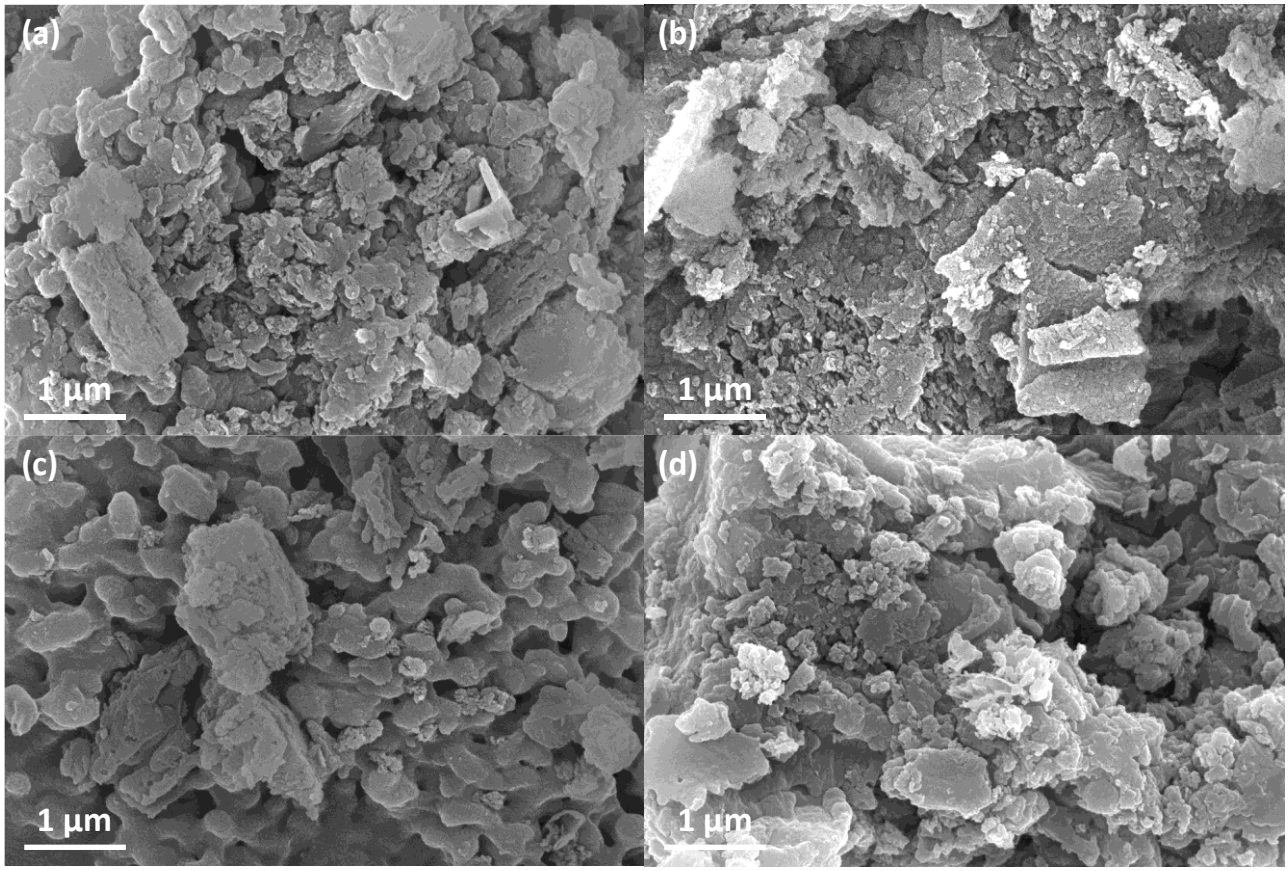

Figure 4. SEM images of PCN-0 (a), PCN-30 Air (b), PCN-30 Ar (c) and PCN-30 Ar-H_2 (d).

The full XPS survey spectra of all the samples (Figure 5(a)) indicate that they are mainly composed of the C element and the N element, as well as a small amount of the O element. The higher intensity of O 1*s* and lower intensity of C 1*s* and N 1*s* of Ar-plasma treated PCN could be caused by the transformation of carbon-containing or nitrogen-containing groups to new active oxygen-containing

species. In the high-resolution XPS spectrum of C 1*s* (Figure 5(b)), two peaks appear at the binding energy of 284.8 eV and 288.2 eV, corresponding to the sp^2 hybridized C–C bond and the N=C–N bond in nitrogen-containing aromatic ring, respectively. The reduction in the peak corresponding to the C–C bond of the plasma-treated PCN in air and Ar-5% H_2 indicates the introduction of carbon vacancies via sputtering. [41]

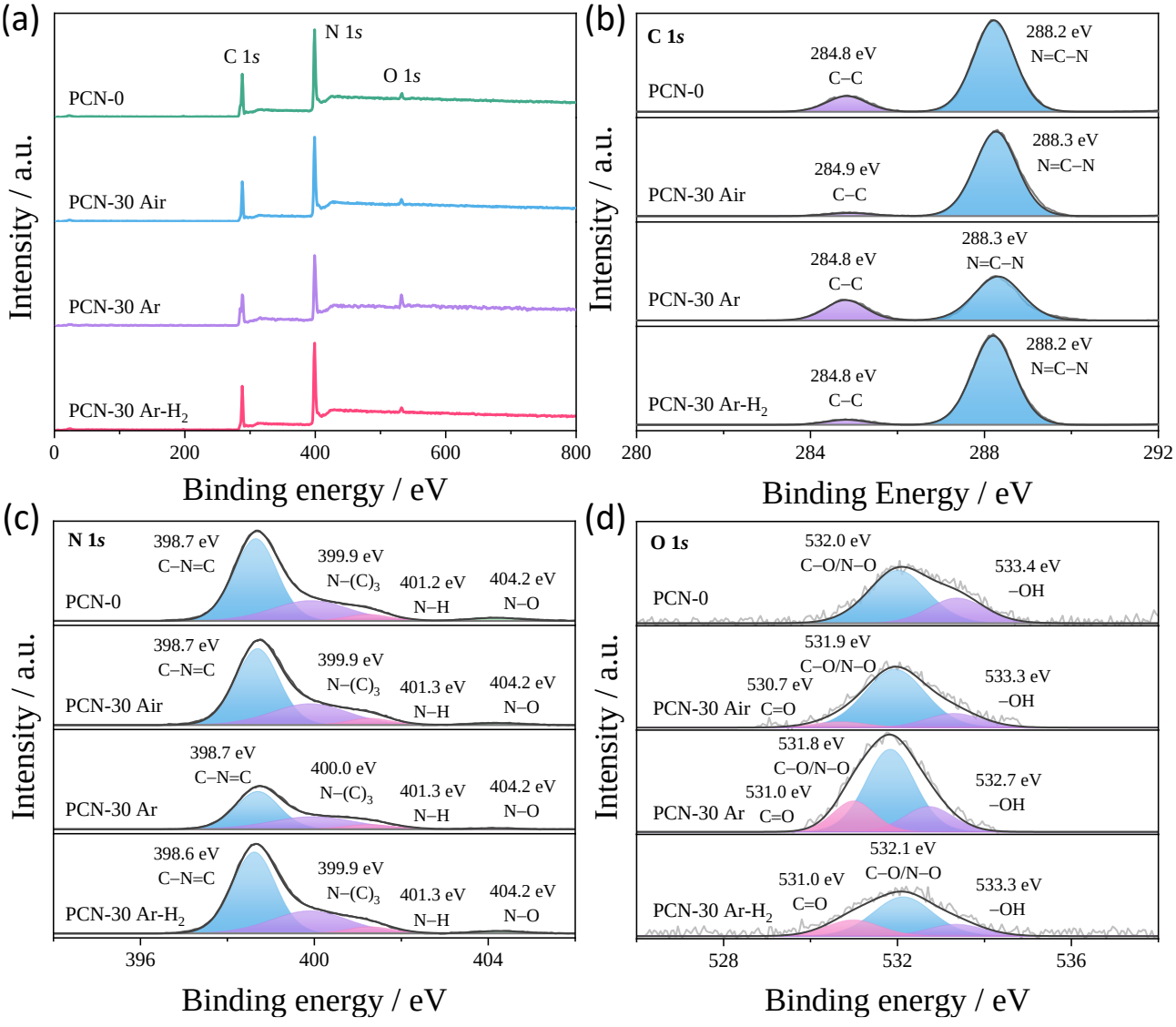

Figure 5. High-resolution XPS spectra for (a) survey, (b) C 1*s*, (c) N 1*s* and (d) O 1*s* of the pristine and plasma-treated PCN.

There are four characteristic peaks in the N 1*s* region (Figure 5(c)) at 398.7, 399.9, 401.2 and 404.2 eV that can be assigned to the sp^2-hybridized aromatic N (C–N=C), tertiary nitrogen (N–$(C)_3$), N in the C–NH_2 structure and oxidized nitrogen (N–O) [42]. In the O 1*s* spectrum (Figure 5(d)), the characteristic peaks at 533.4 eV and 532.0 eV correspond to –OH and C–O or N–O. A new peak for at C=O 530.7 eV was found in the plasma-treated PCN [43]. The increase of C=O indicates the plasma treatment caused the hydrogenation of C–OH [44]. For PCN-30 Ar, the intensity of oxygen-containing groups increases, mainly formed by the reaction between adsorbed water or oxygen on the surface and the active species produced by Ar plasma [45].

The atomic composition from XPS of PCN showed a decreased C/N atomic ratio after the plasma-treated samples in air and Ar-H_2 but an increase in argon (Figure 6(a)). However, the C/N ratio calculated by elemental analysis of the powder by scratching samples was nearly unchanged after plasma (Table S2), indicating that DBD treatment only affected the very surface of the catalysts.

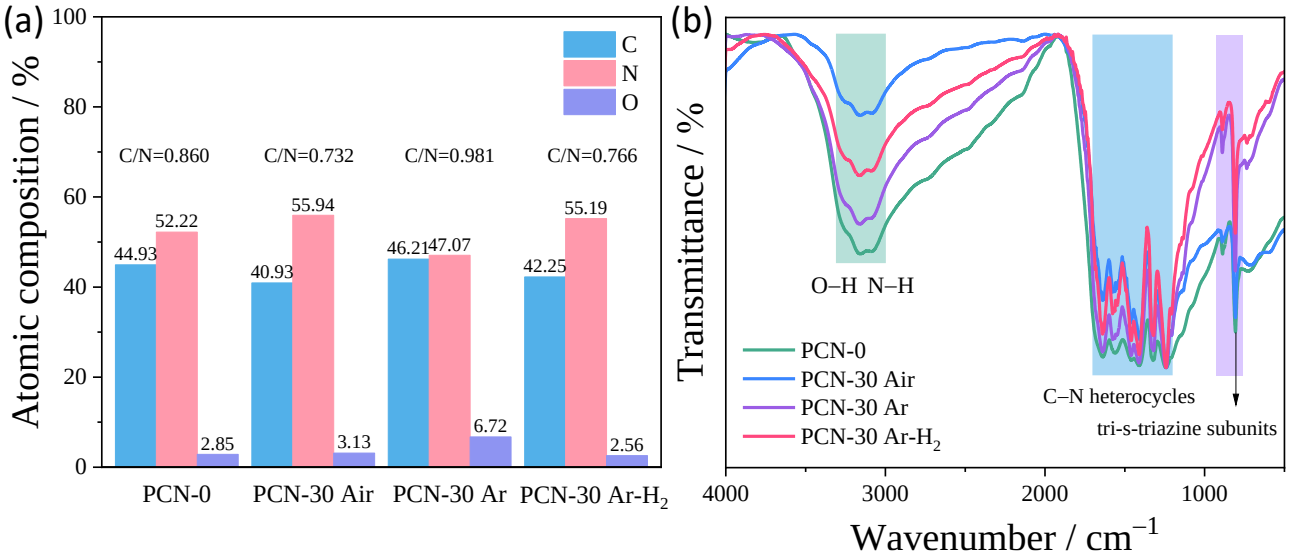

Figure 6. (a) Superficial atomic composition from XPS and (b) FTIR spectra of PCN.

In order to measure the composition and chemical bonding of samples, the FTIR was obtained over

the PCN coating. The O–H and N–H bands in the FTIR spectra (Figure 6(b)) at 3250 cm^{-1} and 3080 cm^{-1} [46] decreased after plasma. The absorption peaks at 1200–1700 cm^{-1} were related to stretching vibrations of the aromatic CN heterocycles [47], while the bands at 1320 cm^{-1} and 1240 cm^{-1} were attributed to the tertiary (N–$(C)_3$) and secondary (N–$(C)_2$) amine fragments [48]. The peaks at 890 cm^{-1} and 810 cm^{-1} belonged to deformation mode of N–H components and vibration of the CN heterocycles for the tri-s-triazine subunits [49].

The TGA curve (Figure S1) indicated that all samples began to lose weight after 500 °C, and the differential TGA (dTG) peaked at 630 °C to 680 °C under flowing air. The thermal stability of plasma treated samples was better than the pristine PCN, which is related to the removal of –OH group that could provide oxygen for the combustion of triazine ring.

3.3. Optical Characterizations

In-situ environmental PL spectrum of samples (Figure 7(a)) at 365 nm under air was used to study the quenching effect of O_2 on the photo-generated electron-hole pairs. The intense and broad PL emission centered at near 468 nm was typical for PCN. [50] The combination of electrons with O_2 would decrease the emission as the consumption of hot charge carriers. The plasma-modified samples showed similar PL spectra to original PCN, whereas their intensities are obviously lower, indicating plasma decreased the recombination of photo-generated electron-hole.

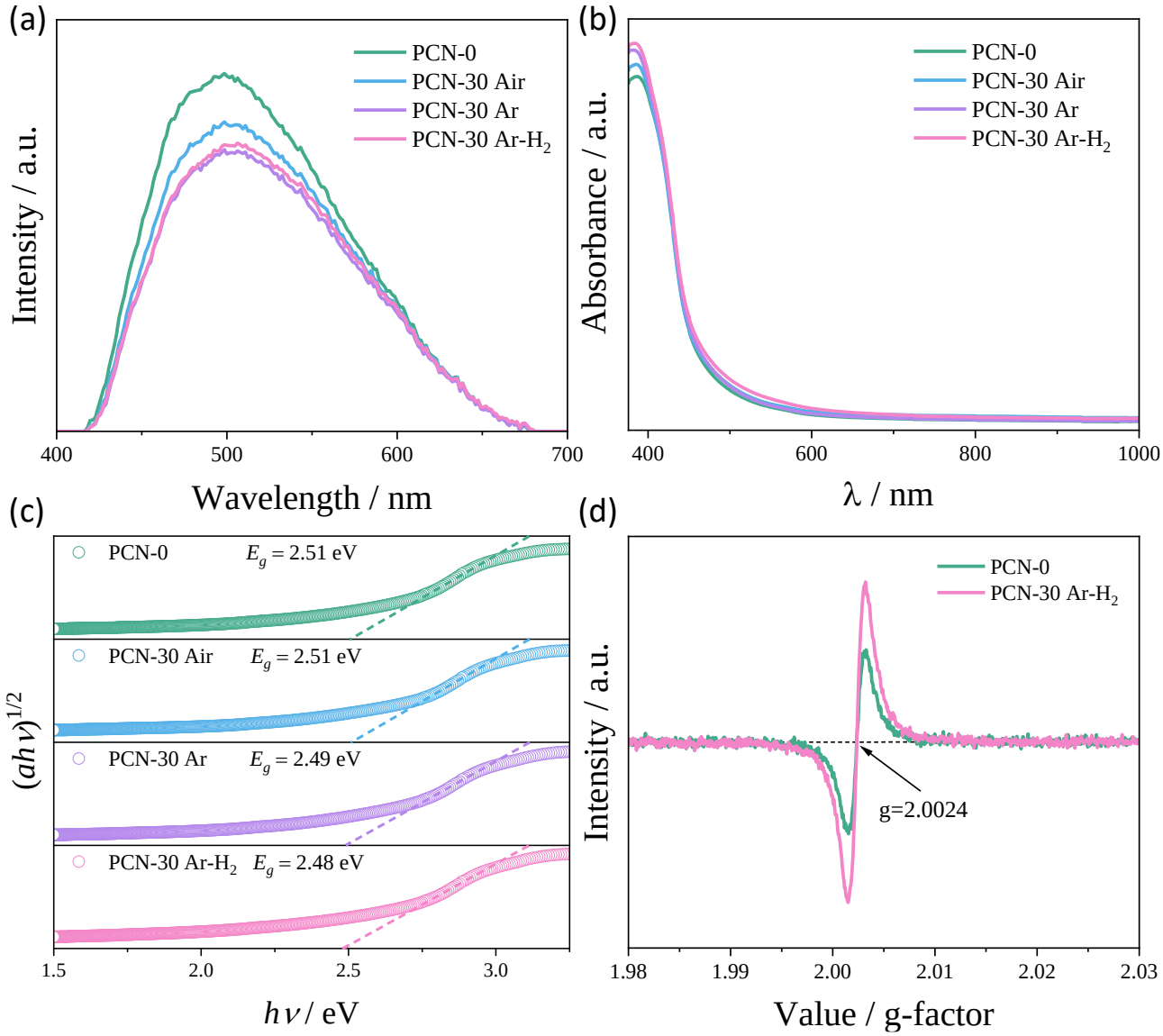

Figure 7. (a) Environmental PL spectra under air; (b) UV-vis diffuse reflectance spectra; (c) tauc plots for an indirect band gap and (d) EPR spectra of PCN.

PCN-0 showed the typical absorption spectrum of graphitic carbon nitride semiconductor with an absorption boundary at about 468 nm [51], and slight red-shift of the absorption bands was observed for modified samples (Figure 7(b)). The forbidden bandwidth of the catalysts is about 2.51 eV calculated by the tauc plot of $(ah\nu)^{1/2}$ vs photon energy (Figure 7(c)), indicating only a short-time discharge treatment results in a lower O-doping content and a lighter physical breakdown between

the layers, which is insufficient to cause a change in the optical band gap of the catalyst. [52]

The EPR spectra (Figure 7(d)) depict that PCN displays a Lorentzian line with the g-factor of 2.0024, stemming from the unpaired electrons on the carbon atoms of the aromatic rings [53]. It is noted that the intensity of EPR signal over the PCN-30 Ar-H_2 is stronger relative to PCN-0, which is attributed to the generation of carbon vacancies improves the efficiency of electron-hole separation [54]. The XPS results also confirmed that carbon vacancy was introduced to PCN-30 in Ar-5% H_2. The increased quantity of unpaired electrons improved the efficiency of photoexcited carrier separation [55].

3.4. Photoelectrochemical measurement

Photoelectrochemical characterization was carried out to further evaluate the charge separation and interfacial charge-transfer properties [56]. The fast photocurrent responses are observed in all the studied electrodes under visible light irradiation (Figure 8(a)). The photocurrent intensity of plasma modified samples is significantly higher than that of PCN-0 (1.19 μA cm^{-2}), indicting the generation of more photoelectrons and the better interfacial charge transfer and higher efficiency in the separation of photoinduced separation of electron-hole pairs after plasma. Furthermore, the decay that appears at the transient photocurrent peak implies a fraction of photogenerated electrons and holes are recombined [57].

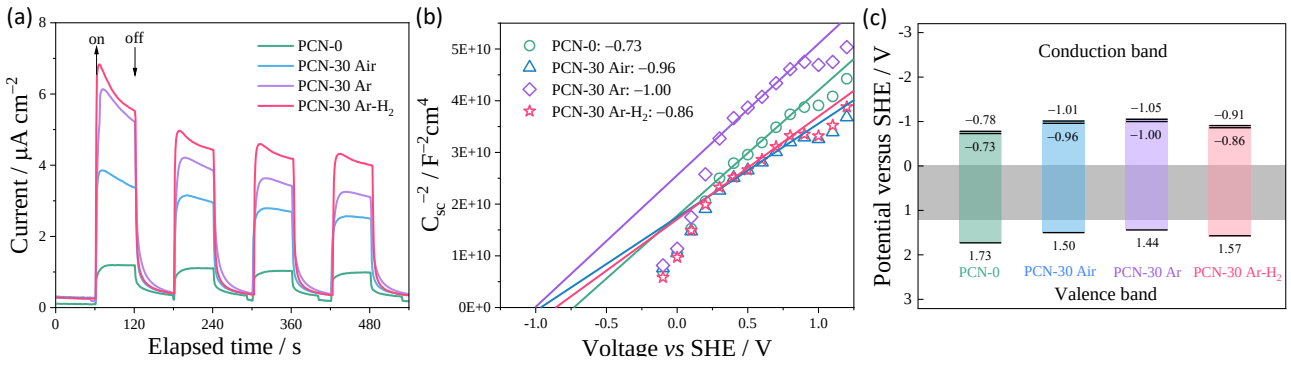

Figure 8. (a) Steady-state chronoamperometry at 0.5 V versus Ag/AgCl reference under dark and illuminated condition; (b) Mott-Schottky plots and (c) the apparent band structure of PCN.

Electrochemical Mott-Schottky test is performed to evaluate the band positions of photocatalysts to confirm the photocatalytic mechanism. The positive slopes of Mott-Schottky results as shown in Figure 8(b) suggest that all samples are typical n-type semiconductors. The flat potentials as represented by the x intercept of the linear region for PCN-0, PCN-30 Air, PCN-30 Ar and PCN-30 Ar-H_2 are estimated to be −0.73 V, −0.96 V, −1.00 V and −0.86 V (vs. SHE). As it is widely accepted, the flat potential of n-type semiconductor is lower 0–0.1 eV than that of the conduction band (CB) potentials. Therefore, the CB potentials are −0.78 V, −1.01 V, −1.05 V and −0.91 V (vs. SHE) as the difference is set as 0.05 eV. The promoted CB maximum position of PCN-30 can provide photogenerated electrons with reductive capability for excellent photocatalytic performance [58]. According to the CB potential and the bandgap values extrapolated by UV-vis spectra, the valence band (VB) potentials are estimated to be 1.73 V, 1.50 V, 1.44 V and 1.57 V (vs. SHE) as shown in Figure 8(c).

3.5. Photocatalytic activity

Figure 9(a) displays the concentration of NO and NO_2 of PCN in air plasma for 10, 30, 60 and 120 minutes, while the measurement with bare quartz (Figure S2) does not show any sign of NO removal. The NO and NO_2 concentration of the plasma-treated PCN suddenly increased in the first 1 minute of the light reaction, but the phenomenon was alleviated with the lapse of time. One reason may be the dissociation of the compound containing N and O produced in air plasma. For another, NO was oxidized to NO_2 by OH. From the results of the FTIR and atomic composition of air plasma, O−H

decreased and O content increased, speculating that N–O adsorbed to produce functional groups. A more severe increase in the content of NOx occurred without NO injecting (Figure 9(b)), suggesting that functional groups were unstable to convert into NO and NO_2 under light.

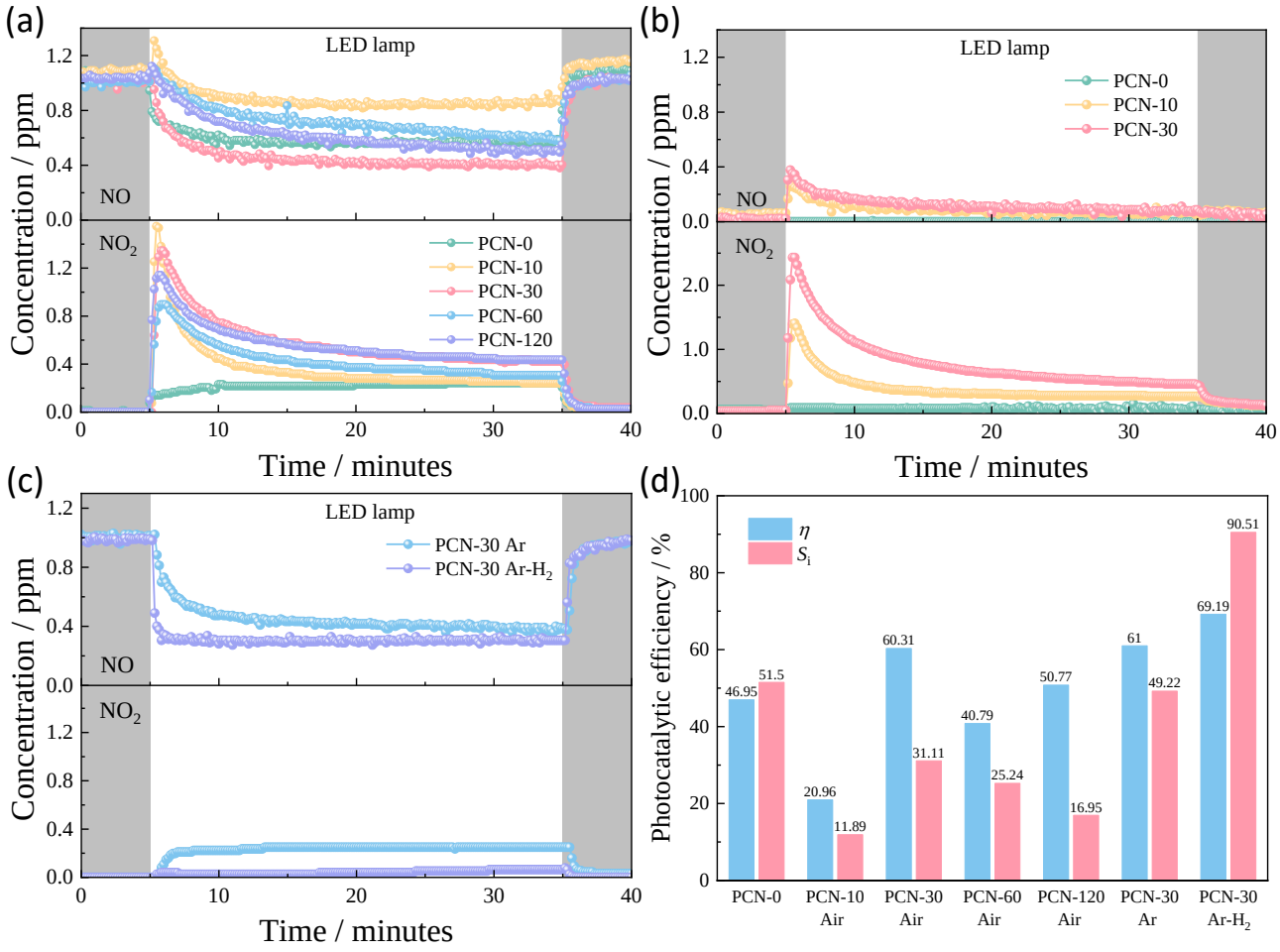

Figure 9. NO removal and NO_2 generation under LED lamp (> 400 nm) of PCN after different duration of plasma treatment in air (a) with or (b) without 1 ppm NO in wet air; (c) NO and NO_2 concentration of PCN treated in Ar and Ar-5% H_2 for 30 minutes under an air flow containing 1 ppm NO; (d) NO removal efficiency (η) and selectivity for ionic species (S_i) of PCN in different conditions.

However, this is not the case in argon and hydrogen plasmas (Figure 9(c)), suggesting that N–O modification have adverse effects on performance. The photocatalytic performance of all

photocatalysts (Figure 9(d)) concluded that the DBD treatment on the surface of PCN can effectively remove NO, especially in Ar-5% H_2, which shows that η increases from the original 46.95% to 69.19% and S_i improves from the original 51.50% to 90.51%. But what we cannot ignore is that the results of air plasma are obtained on the basis of the adverse effects of N−O modification. The photocatalytic stability measurement (Figure S3) showed no obvious decrease in the activity was observed after the cyclic experiments for 3 runs of 30 minutes each, indicating that the plasma-treated PCN exhibit good photocatalytic stability for NO removal under visible light.

4. Discussion

DBD plasma induces surface modification that depends on the gas used for the plasma treatment. A high voltage is applied across the electrodes in the gas to create energetic plasma electrons which are then responsible for the generation of reactive radicals and ions [59, 60]; these plasma species can interact with solid catalysts and reactants. In the emission spectroscopy of air plasma, an obvious NO was found as a result of the activation and reaction between N_2 and O_2. The generation of N atoms is also possible in air plasma [61]. High energy electrons were able to produce NO_3^- or NO_2^- on the surface of ethanol in our previous study [62]. The discharging of air can produce a range of radicals such as OH, H, NO and subsequently lead to the formation of HONO. NO and NO_2 are released by the photodissociation of HONO under illumination [63], which is consistent with the observation of direct emission of NO and NO_2 even in an air flow without NO input:

$$\mathrm{HONO} + h\upsilon \rightarrow \mathrm{NO} + \bullet\,\mathrm{OH} \qquad (3)$$

The presence of NOx related species can also be proven from the omission of initial NO_2 emission after PCN was annealed at 300 °C for 30 minutes after DBD (Figure S4).

OH is clearly present in Ar and Ar-5% H_2 discharges as shown from plasma emission spectroscopy. The relative intensity of the OH band (from XPS and FTIR) in PCN treated in air plasma is much less than the one in pristine PCN and the one treated in Ar and Ar-5% H_2 plasma [64], but extraordinarily high content of nitrogen and oxygen could be related to the adsorbed NOx-related species on the surface during the plasma treatment.

Ionization of Ar gas will produce Ar^+ ions and free electrons due to the plasma glow discharge. The accelerating electric field provides more energy to the free electrons, which effectively reduce NO. Furthermore, Ar^+ ions continuously etch the PCN matrix, resulting in more defects (carbon vacancies) and oxygen-containing groups. Considerable amounts of –OH are presented in electric discharges burning in Ar plasma from spectroscopic analysis, confirming that –OH are also generated by argon plasma [65]. However, In the presence of H_2, the surface –OH bond could react with the H radicals to produce H_2O as a reverse for the production of amine group [66].

In the process of photocatalytic reaction, the electrons on the valence band of PCN are excited under an absorbed photon, leaving a photogenerated electron hole (h^+) on the valence band [67]. Photogenerated carriers can be reacted with O_2 and H_2O to produce active radicals, which oxidize NO and NO_2 (reactions (4)-(9)) [68].

$$h\upsilon \rightarrow e^- + h^+ \quad (4)$$

$$O_2 + e^- \rightarrow \bullet O_2^- \quad (5)$$

$$NO + \bullet O_2^- \rightarrow NO_3^- \quad (6)$$

$$H_2O + h^+ \rightarrow H^+ + \bullet OH \quad (7)$$

$$NO + 2 \bullet OH \rightarrow NO_2 + 2H_2O \quad (8)$$

$$NO_2 + \bullet OH \rightarrow NO_3^- + H^+ \quad (9)$$

The reaction of hot e^- with O_2 would produce $\bullet O_2^-$ for the production of NO_3^-, while the h^+ on the valence band could induce the production of OH radicals for the production NO_2. The high selectivity of PCN-30 Ar and PCN-30 Ar-H_2 for ionic species could be related to the high conduction band that energetically favors the production of reactive oxygen species than the pristine PCN. On the other hand, the poor S_i of PCN-30 Air is ascribed to the adsorption of –NOx on the surface for the production of NO_2, though it also showed higher flat band than the pristine PCN.

5. Conclusion

In summary, a plasma treatment is employed to modify the surface properties of PCN to enhance its visible light photocatalytic performance and sustainability. OES supported the introduction of activity species during plasma treatment. PCN treated in DBD plasma of air, Ar or Ar-5% H_2 showed similar crystal structure than the untreated one but they presented distinct surface than the pristine one depending on the atmosphere. Firstly, plasma treatment generally decreased the surface –OH moieties on PCN that could be reason for the PL emission and increased the –C=O bond. Secondly, the surface defects created *via* plasma treatment effectively suppressed carrier recombination, as indicated by the increased lifetime of PL emission and the stronger EPR intensity. Thirdly, plasma treatment also increased the flat band energy of PCN for the production of a more reducing hot electrons. However, the plasma in air was not suitable for the treatment of PCN because it is able to produce NOx groups that would be released under illumination of visible light. The DBD plasma shows a promise for surface modification and pollutant degradation using plasma-generated active species.

Acknowledgments

This work was supported by Chongqing Science and Technology Committee of China (cstc2021ycjh-bgzxm0162), research funding for central universities of China (SWURC2020002), and EPSRC of UK (EP/R023638/1; EP/M015211/1, EP/K022237/1). Funding from Chongqing Technology and Business University Scientific Research Project (1956017) and the Science and Technology Research Program of Chongqing Municipal Education Commission (Grant No. KJQN201900843) is also acknowledged. Chengsheng Ni also would express gratitude to the award of Chongqing Bayu Young Scholar from Chongqing Teaching Committee and Funding for Oversea Returnees.

References

1. Chen, P.; Liu, H.; Sun, Y.; Li, J.; Cui, W.; Wang, L. a.; Zhang, W.; Yuan, X.; Wang, Z.; Zhang, Y.; Dong, F., Bi metal prevents the deactivation of oxygen vacancies in Bi2O2CO3 for stable and efficient photocatalytic NO abatement. *Applied Catalysis B-Environmental* **2020,** *264*.

2. Zhou, Y.; Zhao, Z.; Wang, F.; Cao, K.; Doronkin, D. E.; Dong, F.; Grunwaldt, J.-D., Facile synthesis of surface N-doped $Bi_2O_2CO_3$: Origin of visible light photocatalytic activity and in situ DRIFTS studies. *J. Hazard. Mater.* **2016,** *307*, 163-172.

3. Xue, W.; Huang, D.; Wen, X.; Chen, S.; Cheng, M.; Deng, R.; Li, B.; Yang, Y.; Liu, X., Silver-based semiconductor Z-scheme photocatalytic systems for environmental purification. *Journal of Hazardous Materials* **2020,** *390*.

4. Cao, S.; Low, J.; Yu, J.; Jaroniec, M., Polymeric Photocatalysts Based on Graphitic Carbon Nitride. *Advanced Materials* **2015,** *27* (13), 2150-2176.

5. Akhundi, A.; Habibi-Yangjeh, A.; Abitorabi, M.; Pouran, S. R., Review on photocatalytic conversion of carbon dioxide to value-added compounds and renewable fuels by graphitic carbon nitride-based photocatalysts. *Catal. Rev.-Sci. Eng.* **2019,** *61* (4), 595-628.

6. Xiong, T.; Cen, W. L.; Zhang, Y. X.; Dong, F., Bridging the g-C3N4 Interlayers for Enhanced Photocatalysis. *Acs Catalysis* **2016,** *6* (4), 2462-2472.

7. Kang, Y. Y.; Yang, Y. Q.; Yin, L. C.; Kang, X. D.; Wang, L. Z.; Liu, G.; Cheng, H. M., Selective Breaking of Hydrogen Bonds of Layered Carbon Nitride for Visible Light Photocatalysis. *Advanced Materials* **2016,** *28* (30), 6471-+.

8. Bai, X. J.; Zong, R. L.; Li, C. X.; Liu, D.; Liu, Y. F.; Zhu, Y. F., Enhancement of visible photocatalytic activity via Ag@C3N4 core-shell plasmonic composite. *Applied Catalysis B-Environmental* **2014,** *147*, 82-91.

9. Li, K. L.; Cui, W.; Li, J. Y.; Sun, Y. J.; Chu, Y. H.; Jiang, G. M.; Zhou, Y.; Zhang, Y. X.; Dong, F., Tuning the reaction pathway of photocatalytic NO oxidation process to control the secondary pollution on monodisperse Au nanoparticles@g-C3N4. *Chemical Engineering Journal* **2019,** *378*, 9.

10. Li, Y. H.; Sun, Y. J.; Ho, W. K.; Zhang, Y. X.; Huang, H. W.; Cai, Q.; Dong, F., Highly enhanced visible-light photocatalytic NOx purification and conversion pathway on self-structurally modified g-C3N4 nanosheets. *Science Bulletin* **2018,** *63* (10), 609-620.

11. Dong, F.; Li, Y. H.; Wang, Z. Y.; Ho, W. K., Enhanced visible light photocatalytic activity and oxidation ability of porous graphene-like g-C3N4 nanosheets via thermal exfoliation. *Applied Surface Science* **2015,** *358*, 393-403.

12. Li, S. N.; Dong, G. H.; Hailili, R.; Yang, L. P.; Li, Y. X.; Wang, F.; Zeng, Y. B.; Wang, C. Y., Effective photocatalytic H2O2 production under visible light irradiation at g-C3N4 modulated by carbon vacancies. *Applied Catalysis B-Environmental* **2016,** *190*, 26-35.

13. Vinchon, P.; Glad, X.; Bigras, G. R.; Martel, R.; Stafford, L., Preferential self-healing at grain boundaries in plasma-treated graphene. *Nat. Mater.* **2021,** *20* (1), 49-54.

14. Wang, C.; Fu, M.; Cao, J.; Wu, X. L.; Hu, X. L.; Dong, F., BaWO4/g-C3N4 heterostructure with excellent bifunctional photocatalytic performance. *Chemical Engineering Journal* **2020,** *385*, 11.

15. Pham, V. V.; Mai, D. Q.; Bui, D. P.; Man, T. V.; Zhu, B. C.; Zhang, L. Y.; Sangkaworn, J.; Tantirungrotechai, J.; Reutrakul, V.; Cao, T. M., Emerging 2D/0D g-C3N4/SnO2 S-scheme photocatalyst: New generation architectural structure of heterojunctions toward visible-light-driven NO degradation star. *Environ. Pollut.* **2021,** *286*, 11.

16. Van Pham, V.; Truong, T. K.; Le, H. V.; Nguyen, H. T.; Tong, H. D.; Cao, T. M., Enhancing Green Product Generation of Photocatalytic NO Oxidation: A Case of WO3 Nanoplate/g-C3N4 S-Scheme Heterojunction. *Langmuir : the ACS journal of surfaces and colloids* **2022,** *38* (13), 4138-4146.

17. Zhao, Y.; Zhao, F.; Wang, X. P.; Xu, C. Y.; Zhang, Z. P.; Shi, G. Q.; Qu, L. T., Graphitic Carbon Nitride Nanoribbons: Graphene-Assisted Formation and Synergic Function for Highly Efficient Hydrogen Evolution. *Angewandte Chemie-International Edition* **2014,** *53* (50), 13934-13939.

18. Giannakopoulou, T.; Papailias, I.; Todorova, N.; Boukos, N.; Liu, Y.; Yu, J. G.; Trapalis, C., Tailoring the energy band gap and edges' potentials of g-C3N4/TiO2 composite photocatalysts for NOx removal. *Chemical Engineering Journal* **2017,** *310*, 571-580.

19. Seo, H. K.; Elliott, C. M.; Shin, H. S., Mesoporous TiO2 Films Fabricated Using Atmospheric Pressure Dielectric Barrier Discharge Jet. *Acs Applied Materials & Interfaces* **2010,** *2* (12), 3397-3400.

20. Li, X.; Zhang, J.; Zhou, F.; Zhang, H.; Bai, J.; Wang, Y.; Wang, H., Preparation of N-vacancy-doped g-C3N4 with outstanding photocatalytic H2O2 production ability by dielectric barrier discharge plasma treatment. *Chinese Journal of Catalysis* **2018,** *39* (6), 1090-1098.

21. Ma, L.; Hu, S.; Li, P.; Wang, Q.; Ma, H.; Li, W., In situ synthesis of sulfur doped carbon nitride with enhanced photocatalytic performance using DBD plasma treatment under H2S atmosphere. *J. Phys. Chem. Solids* **2018,** *118*, 166-171.

22. Sprick, R. S.; Cheetham, K. J.; Bai, Y.; Fernandes, J. A.; Barnes, M.; Bradley, J. W.; Cooper, A. I., Polymer photocatalysts with plasma-enhanced activity. *Journal of Materials Chemistry A* **2020,** *8* (15), 7125-7129.

23. Kong, X. C.; Xu, Y. M.; Cui, Z. D.; Li, Z. Y.; Liang, Y. Q.; Gao, Z. H.; Zhu, S. L.; Yang, X. J., Defect enhances photocatalytic activity of ultrathin TiO2 (B) nanosheets for hydrogen production by plasma engraving method. *Applied Catalysis B-Environmental* **2018,** *230*, 11-17.

24. Luo, Z. W.; Jiang, H.; Hu, L. Z.; Li, D.; Geng, W. H.; Wei, P., Effect of N-2/Ar plasma treatment on the visible light photocatalytic activity of CuO/TiO2. *Chinese Journal of Catalysis* **2014,** *35* (10), 1752-1760.

25. Bootluck, W.; Chittrakarn, T.; Techato, K.; Khongnakorn, W., Modification of surface alpha-Fe2O3/TiO2 photocatalyst nanocomposite with enhanced photocatalytic activity by Ar gas plasma treatment for hydrogen evolution. *Journal of Environmental Chemical Engineering* **2021,** *9* (4), 11.

26. Lu, N.; Liu, N.; Hui, Y.; Shang, K. F.; Jiang, N.; Li, J.; Wu, Y., Characterization of highly effective plasma-treated g-C3N4 and application to the photocatalytic H2O2 production. *Chemosphere* **2020,** *241*, 10.
27. Ma, J.; Wang, C.; He, H., Enhanced photocatalytic oxidation of NO over g-C3N4-TiO2 under UV and visible light. *Applied Catalysis B: Environmental* **2016,** *184*, 28-34.
28. Abdellatif, H. R. S.; Zhang, G.; Tang, Y.; Ruan, W. J.; Li, J. B.; Xie, D. T.; Ni, J. P.; Ni, C. S., A highly efficient dual-phase GaN(O)/Nb2O5(N) photocatalyst prepared through nitridation and reoxidation process for NO removal. *Chemical Engineering Journal* **2020,** *402*, 11.
29. Yang, M.; Liu, K.; Ma, L. H.; Cheong, K. P.; Wang, Z.; Ho, W. K.; Ren, W., Time-resolved characterization of non-thermal plasma-assisted photocatalytic removal of nitric oxide. *Journal of Physics D-Applied Physics* **2020,** *53* (1), 7.
30. Gorjanc, M.; Mozetič, M.; Primc, G.; Vesel, A.; Spasić, K.; Puač, N.; Petrović, Z. L.; Kert, M., Plasma treated polyethylene terephthalate for increased embedment of UV-responsive microcapsules. *Applied Surface Science* **2017,** *419*, 224-234.
31. Moshkalyov, S. A.; Steen, P. G.; Gomez, S.; Graham, W. G., Role of low-energy electrons in Ar emission from low-pressure radio frequency discharge plasma. *Appl. Phys. Lett.* **1999,** *75* (3), 328-330.
32. Sasaki, K.; Wakasaki, T.; Kadota, K., Observation of continuum optical emission from laser-ablation carbon plumes. *Applied Surface Science* **2002,** *197*, 197-201.
33. Dorn, H. P.; Neuroth, R.; Hofzumahaus, A., INVESTIGATION OF OH ABSORPTION CROSS-SECTIONS OF ROTATIONAL TRANSITIONS IN THE A(2)SIGMA(+), V'=0 - X(2)PI, V''=0 BAND UNDER ATMOSPHERIC CONDITIONS - IMPLICATIONS FOR TROPOSPHERIC LONG-PATH ABSORPTION-MEASUREMENTS. *Journal of Geophysical Research-Atmospheres* **1995,** *100* (D4), 7397-7409.
34. Wei, Z.; Liu, M. L.; Zhang, Z. J.; Yao, W. Q.; Tan, H. W.; Zhu, Y. F., Efficient visible-light-driven selective oxygen reduction to hydrogen peroxide by oxygen-enriched graphitic carbon nitride polymers. *Energy Environ. Sci.* **2018,** *11* (9), 2581-2589.
35. Fu, J.; Yu, J.; Jiang, C.; Cheng, B., g-C3N4-Based Heterostructured Photocatalysts. *Advanced Energy Materials* **2018,** *8* (3).
36. Jiang, L.-L.; Wang, Z.-K.; Li, M.; Zhang, C.-C.; Ye, Q.-Q.; Hu, K.-H.; Lu, D.-Z.; Fang, P.-F.; Liao, L.-S., Passivated Perovskite Crystallization via g-C3N4 for High-Performance Solar Cells. *Advanced Functional Materials* **2018,** *28* (7).
37. Zeng, Z. X.; Yu, H. T.; Quan, X.; Chen, S.; Zhang, S. S., Structuring phase junction between tri-s-triazine and triazine crystalline C3N4 for efficient photocatalytic hydrogen evolution. *Applied Catalysis B-Environmental* **2018,** *227*, 153-160.
38. Hu, X. L.; Zhang, W. J.; Yong, Y. W.; Xu, Y.; Wang, X. H.; Yao, X. X., One-step synthesis of iodine-doped g-C3N4 with enhanced photocatalytic nitrogen fixation performance. *Applied Surface Science* **2020,** *510*, 7.
39. Abdellatif, H. R. S.; Zhang, G.; Wang, X.; Xie, D.; Irvine, J. T. S.; Ni, J.; Ni, C., Boosting photocatalytic oxidation on graphitic carbon nitride for efficient photocatalysis by heterojunction with graphitic carbon units. *Chem. Eng. J. (Lausanne)* **2019,** *370*, 875-884.
40. Fina, F.; Callear, S. K.; Carins, G. M.; Irvine, J. T. S., Structural Investigation of Graphitic Carbon Nitride via XRD and Neutron Diffraction. *Chemistry of Materials* **2015,** *27* (7), 2612-2618.
41. Li, J. X.; Ma, W. Q.; Chen, J. J.; An, N.; Zhao, Y.; Wang, D. J.; Mao, Z. Y., Carbon vacancies improved photocatalytic hydrogen generation of g-C3N4 photocatalyst via magnesium vapor etching. *International Journal of Hydrogen Energy* **2020,** *45* (27), 13939-13946.
42. Gorgulho, H. F.; Goncalves, F.; Pereira, M. F. R.; Figueiredo, J. L., Synthesis and characterization of nitrogen-

doped carbon xerogels. *Carbon* **2009,** *47* (8), 2032-2039.

43. Gargiulo, V.; Alfano, B.; Di Capua, R.; Alfe, M.; Vorokhta, M.; Polichetti, T.; Massera, E.; Miglietta, M. L.; Schiattarella, C.; Di Francia, G., Graphene-like layers as promising chemiresistive sensing material for detection of alcohols at low concentration. *J. Appl. Phys.* **2018,** *123* (2), 8.

44. Korstanje, T. J.; van der Vlugt, J. I.; Elsevier, C. J.; de Bruin, B., Hydrogenation of carboxylic acids with a homogeneous cobalt catalyst. *Science* **2015,** *350* (6258), 298-+.

45. Ding, J. J.; Sun, X. X.; Wang, Q.; Li, D. S.; Li, X. Y.; Li, X. X.; Chen, L.; Zhang, X.; Tian, X. Y.; Ostrikov, K., Plasma synthesis of Pt/g-C3N4 photocatalysts with enhanced photocatalytic hydrogen generation. *Journal of Alloys and Compounds* **2021,** *873*, 10.

46. Wang, J.; Wang, Y.; Wang, W.; Ding, Z.; Geng, R.; Li, P.; Pan, D.; Liang, J.; Qin, H.; Fan, Q., Tunable mesoporous g-C3N4 nanosheets as a metal-free catalyst for enhanced visible-light-driven photocatalytic reduction of U(VI). *Chemical Engineering Journal* **2020,** *383*, 123193.

47. Feng, D.; Cheng, Y.; He, J.; Zheng, L.; Shao, D.; Wang, W.; Wang, W.; Lu, F.; Dong, H.; Liu, H.; Zheng, R.; Liu, H., Enhanced photocatalytic activities of g-C3N4 with large specific surface area via a facile one-step synthesis process. *Carbon* **2017,** *125*, 454-463.

48. Hu, R.; Wang, X.; Dai, S.; Shao, D.; Hayat, T.; Alsaedi, A., Application of graphitic carbon nitride for the removal of Pb(II) and aniline from aqueous solutions. *Chemical Engineering Journal* **2015,** *260*, 469-477.

49. Zhang, J.; Zhang, M.; Lin, L.; Wang, X., Sol Processing of Conjugated Carbon Nitride Powders for Thin-Film Fabrication. *Angewandte Chemie-International Edition* **2015,** *54* (21), 6297-6301.

50. Oveisi, M.; Mahmoodi, N. M.; Asli, M. A., Facile and green synthesis of metal-organic framework/inorganic nanofiber using electrospinning for recyclable visible-light photocatalysis. *Journal of Cleaner Production* **2019,** *222*, 669-684.

51. Liu, J.; Liu, Y.; Liu, N.; Han, Y.; Zhang, X.; Huang, H.; Lifshitz, Y.; Lee, S.-T.; Zhong, J.; Kang, Z., Metal-free efficient photocatalyst for stable visible water splitting via a two-electron pathway. *Science* **2015,** *347* (6225), 970-974.

52. Mao, Z.; Chen, J.; Yang, Y.; Bie, L.; Fahlman, B. D.; Wang, D., Modification of surface properties and enhancement of photocatalytic performance for g-C3N4 via plasma treatment. *Carbon* **2017,** *123*, 651-659.

53. Li, Y. H.; Gu, M. L.; Shi, T.; Cui, W.; Zhang, X. M.; Dong, F.; Cheng, J. S.; Fan, J. J.; Lv, K. L., Carbon vacancy in C3N4 nanotube: Electronic structure, photocatalysis mechanism and highly enhanced activity. *Applied Catalysis B-Environmental* **2020,** *262*, 11.

54. Liang, Q. H.; Li, Z.; Huang, Z. H.; Kang, F. Y.; Yang, Q. H., Holey Graphitic Carbon Nitride Nanosheets with Carbon Vacancies for Highly Improved Photocatalytic Hydrogen Production. *Advanced Functional Materials* **2015,** *25* (44), 6885-6892.

55. Wang, X. W.; Li, Q. C.; Gan, L.; Ji, X. F.; Chen, F. Y.; Peng, X. K.; Zhang, R. B., 3D macropore carbon-vacancy g-C3N4 constructed using polymethylmethacrylate spheres for enhanced photocatalytic H-2 evolution and CO2 reduction. *J. Energy Chem.* **2021,** *53*, 139-146.

56. Zhu, Z.; Huo, P.; Lu, Z.; Yan, Y.; Liu, Z.; Shi, W.; Li, C.; Dong, H., Fabrication of magnetically recoverable photocatalysts using g-C3N4 for effective separation of charge carriers through like-Z-scheme mechanism with Fe3O4 mediator. *Chemical Engineering Journal* **2018,** *331*, 615-625.

57. Ye, L.; Chen, S., Fabrication and high visible-light-driven photocurrent response of g-C3N4 film: The role of thiourea. *Applied Surface Science* **2016,** *389*, 1076-1083.

58. Meng, N. N.; Ren, J.; Liu, Y.; Huang, Y.; Petit, T.; Zhang, B., Engineering oxygen-containing and amino groups into two-dimensional atomically-thin porous polymeric carbon nitrogen for enhanced photocatalytic

hydrogen production. *Energy Environ. Sci.* **2018,** *11* (3), 566-571.
59. Wang, X.; Chen, Y.; Fu, M.; Chen, Z.; Huang, Q., Effect of high-voltage discharge non-thermal plasma on g-C3N4 in a plasma-photocatalyst system. *Chinese Journal of Catalysis* **2018,** *39* (10), 1672-1682.
60. Bogaerts, A.; Tu, X.; Whitehead, J. C.; Centi, G.; Lefferts, L.; Guaitella, O.; Azzolina-Jury, F.; Kim, H. H.; Murphy, A. B.; Schneider, W. F.; Nozaki, T.; Hicks, J. C.; Rousseau, A.; Thevenet, F.; Khacef, A.; Carreon, M., The 2020 plasma catalysis roadmap. *Journal of Physics D-Applied Physics* **2020,** *53* (44), 51.
61. Takamatsu, T.; Uehara, K.; Sasaki, Y.; Miyahara, H.; Matsumura, Y.; Iwasawa, A.; Ito, N.; Azuma, T.; Kohno, M.; Okino, A., Investigation of reactive species using various gas plasmas. *Rsc Advances* **2014,** *4* (75), 39901-39905.
62. Ni, C. S.; Carolan, D.; Rocks, C.; Hui, J. N.; Fang, Z. G.; Padmanaban, D. B.; Ni, J. P.; Xie, D. T.; Maguire, P.; Irvine, J. T. S.; Mariotti, D., Microplasma-assisted electrochemical synthesis of Co3O4 nanoparticles in absolute ethanol for energy applications. *Green Chemistry* **2018,** *20* (9), 2101-2109.
63. Gu, R. R.; Shen, H. Q.; Xue, L. K.; Wang, T.; Gao, J.; Li, H.; Liang, Y. T.; Xia, M.; Yu, C.; Liu, Y. M.; Wang, W. X., Investigating the sources of atmospheric nitrous acid (HONO) in the megacity of Beijing, China. *Science of the Total Environment* **2022,** *812*, 10.
64. Tampieri, F.; Ginebra, M. P.; Canal, C., Quantification of Plasma-Produced Hydroxyl Radicals in Solution and their Dependence on the pH. *Anal. Chem.* **2021,** *93* (8), 3666-3670.
65. Benstaali, B.; Boubert, P.; Cheron, B. G.; Addou, A.; Brisset, J. L., Density and rotational temperature measurements of the OH degrees and NO degrees radicals produced by a gliding arc in humid air. *Plasma Chemistry and Plasma Processing* **2002,** *22* (4), 553-571.
66. Guo, H.; Jiang, N.; Wang, H. J.; Shang, K. F.; Lu, N.; Li, J.; Wu, Y., Enhanced catalytic performance of graphene-TiO2 nanocomposites for synergetic degradation of fluoroquinolone antibiotic in pulsed discharge plasma system. *Applied Catalysis B-Environmental* **2019,** *248*, 552-566.
67. Martha, S.; Nashim, A.; Parida, K. M., Facile synthesis of highly active g-C3N4 for efficient hydrogen production under visible light. *Journal of Materials Chemistry A* **2013,** *1* (26), 7816-7824.
68. Wang, X.; Ren, Y.; Li, Y.; Zhang, G., Fabrication of 1D/2D BiPO4/g-C3N4 heterostructured photocatalyst with enhanced photocatalytic efficiency for NO removal. *Chemosphere* **2022,** *287*, 132098.